Mechanism Insights of Ethane C−H Bond Activations by Bare [Fe−III=O](+): Explicit Electronic Structure Analysis

ARTICLE *in* THE JOURNAL OF PHYSICAL CHEMISTRY A · FEBRUARY 2012

Impact Factor: 2.69 · DOI: 10.1021/jp2120302 · Source: PubMed

5 AUTHORS, INCLUDING:

Xiaoli Sun
Jilin University
9 PUBLICATIONS **46** CITATIONS
SEE PROFILE

Dan Mu
Jilin University
166 PUBLICATIONS **1,138** CITATIONS
SEE PROFILE

Jilai Li
Jilin University
66 PUBLICATIONS **287** CITATIONS
SEE PROFILE

THE JOURNAL OF PHYSICAL CHEMISTRY A

Article

pubs.acs.org/JPCA

Mechanism Insights of Ethane C−H Bond Activations by Bare $[Fe^{III}{=}O]^+$: Explicit Electronic Structure Analysis

Xiao-Li Sun,[‡] Xu-Ri Huang,[‡] Ji-Lai Li,*[,‡,†] Rui-Ping Huo,[‡] and Chia-Chung Sun[‡]

[‡]State Key Laboratory of Theoretical and Computational Chemistry, Institute of Theoretical Chemistry, Jilin University, Changchun 130023, People's Republic of China

[†]Department of Theoretical Chemistry, Lund University, Chemical Centre, P.O. Box 124, SE-221 00 Lund, Sweden

Supporting Information

ABSTRACT: Alkane C−H bond activation by various catalysts and enzymes has attracted considerable attention recently, but many issues are still unanswered. The conversion of ethane to ethanol and ethene by bare $[Fe^{III}{=}O]^+$ has been explored using density functional theory and coupled-cluster method comprehensively. Two possible reaction mechanisms are available for the entire reaction, the direct H-abstraction mechanism and the concerted mechanism. First, in the direct H-abstraction mechanism, a direct H-abstraction is encountered in the initial step, going through a collinear transition state C···H···O−Fe and then leading to the generation of an intermediate Fe−OH bound to the alkyl radical weakly. The final product of the direct H-abstraction mechanism is ethanol, which is produced by the hydroxyl group back transfer to the carbon radical. Second, in the concerted reaction mechanism, the H-abstraction process is characterized via overcoming four/five-centered transition states $^{6/4}$TSH_c5 or ^{4}TSH_c4. The second step of the concerted mechanism can lead to either product ethanol or ethene. Moreover, the major product ethene can be obtained through two different pathways, the one-step pathway and the stepwise pathway. It is the first report that the former pathway starting from $^{6/4}$IM_c to the product can be better described as a proton-coupled electron transfer (PCET). It plays an important role in the product ethene generation according to the CCSD(T) results. The spin−orbital coupling (SOC) calculations demonstrate that the title reaction should proceed via a two-state reactivity (TSR) pattern and that the spin-forbidden transition could slightly lower the rate-determining energy barrier height. This thorough theoretical study, especially the explicit electronic structure analysis, may provide important clues for understanding and studying the C−H bond activation promoted by iron-based artificial catalysts.

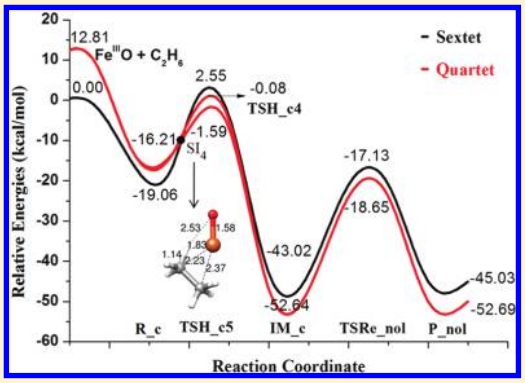

1. INTRODUCTION

The hydroxylation of hydrocarbon C−H bonds is a very difficult transformation. Nevertheless, the C−H hydroxylation reactions are catalyzed effectively and deftly by a variety of metalloenzymes under physiological conditions, among which the most diverse are the many members of the cytochrome P450 family.[1−12] Two well-known examples are the alkane hydroxylation by cytochrome P450 and nonheme iron(IV)−oxo complexes, which were investigated by Shaik,[4,7,12−19] Solomon,[20−23] Que,[20,24,25] Thiel,[26−30] Siegbahn,[31,32] Neese,[33−35] de Visser,[36−43] Baerends,[44,45] and Schwarz[46,47] and co-workers extensively. Interestingly, both the heme species in cytochrome P450 and nonheme species in nature and biomimetic systems share similar mechanistic features in C−H bond hydroxylation. The well-accepted enzymatic catalysis mechanism is better described as follows (Scheme 1):[1,3,18,39,41,42,48−52] (a) Hydrogen−atom abstraction from the substrate R−H, which leads to the iron(III)-hydroxyl center weakly bound to the alkyl radical R• (hydrogen-atom transfer, HAT) and (b) hydroxyl rebounding to the substrate radical R• to yield an iron(II) center, resulting in the hydroxylated product R−OH (O-rebound). Clearly, this is characteristic of a stepwise mechanism that involves two-electron reduction to the iron(IV) center.

Scheme 1

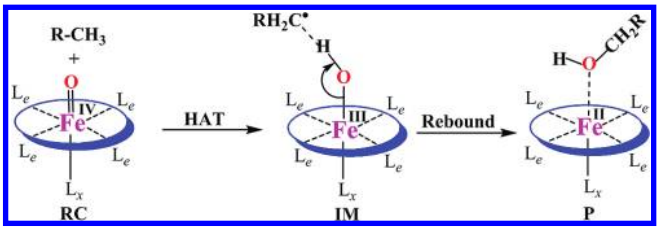

Contrary to the functionalization of the unactivated C−H bond in nature, the effective C−H bond activation under mild conditions in catalytic chemistry has been a long-standing goal and challenge for human beings. Specifically, the selective

Received: December 13, 2011
Revised: January 11, 2012
Published: January 12, 2012

oxidation of the C−H bond in hydrocarbons by transition metals has attracted great attention because they can be viewed as a model for both biological metabolism processes and modern catalytic chemistry.[5,8,53−58] In addition, the majority of model complexes prefer the low spin (LS) states,[40,59−61] whereas all of the identified nonheme iron enzyme active sites feature the high spin (HS) ones.[17,33,34,62] Studies on the gas-phase reactions of bare transition-metal ions and hydrocarbons provided a wealth of insight concerning on the intrinsic interactions between the active sites of catalysts and organic substrates. With respect to biological relevance, the gas-phase C−H bond activations of small hydrocarbons by various transition-metal oxides were investigated by Schwarz, Freiser, and co-workers 20 years ago.[63,64] It was demonstrated that gas-phase bare $[FeO]^+$ can directly convert methane to methanol and ethane to ethylene and/or ethanol effectively at room temperature. A nonradical, two-step reaction mechanism for methane hydroxylation by the bare $[FeO]^+$ complex and soluble methane monooxygenase was proposed from quantum chemical calculations.[65] The ethane oxidation by FeO^+ is analogous to that of methane except that the channel represented by the formation of C_2H_5OH becomes less competitive. The direct insertion of the FeO group into the C−H bond was envisioned as occurring via a four-centered intermediate, and initial insertion of Fe followed by hydrogen migration onto the oxygen might exist (Scheme 2).[66−68] The

Scheme 2

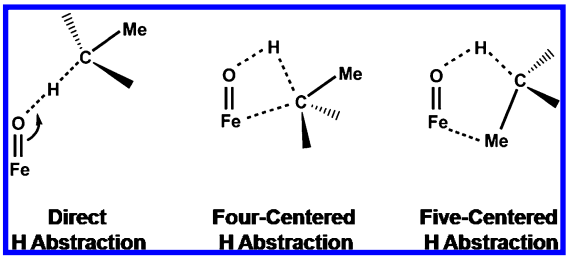

thermochemically favored elimination of H_2O to produce C_2H_4 is dominant.[69−71] By a detailed analysis of the gas-phase reactions between this simple, diatomic reagent $[FeO]^+$ and H_2/CH_4, the concept of two-state reactivity (TSR)[72] was well-established.[73] Henceforth, extensive studies have been executed by experimental methods as well as theoretical studies on simple model systems, such as alkanes, alkenes, and benzene with transition-metal oxides.[64,74] Being viewed as the simplest model for alkane hydroxylation, Yoshizawa and Kulik conducted a series of work to investigate the methane to methanol conversion by first-row transition-metal oxide ions with different charges.[65−68,75−86] They found that the concerted H-atom abstraction via a four-centered transition state is energetically more favorable than the direct H-atom abstraction via a transition state with a collinear C−H−O array, and the iron(IV)−oxo complexes appeared to be the most effective catalyst toward C−H bond activation. On the basis of advanced gas-phase spectroscopy combined with rather high level calculations, a complete description of the gas-phase conversion of methane to methanol by $[FeO]^+$ was established very recently.[87] In addition, Baerends et al. also investigated the solvent effect for reaction of methane and methanol conversion by $[Fe{=}O]^{2+}$.[45]

As a model substrate, ethane hydroxylation by Cpd I and nonheme iron(IV)−oxo complexes has been investigated theoretically.[17,33,42] In addition, theoretical investigation of ethane oxidation by $[Fe{=}O]^+$ was reported recently by Zhao and co-workers at the B3LYP level (Fe, DZVP; nonmetal atoms, 6-311+G(2d,2p)) on the basis of experimental study.[88] In their work, (1) no classical O-rebound mechanism following the H-abstraction was found; (2) the four-centered process did not exist, which is preferred at a coordinatively unsaturated metal center as proposed by Yoshizawa; and (3) the electronic transfer behavior was unclear. These issues stimulated our impetus, and we therefore revisited this key reaction. Clearly, the catalysis of ethane by bare FeO^+ offers a rich and complex mechanistic puzzle. This reaction represents a paradigmatic, challenging test case for electronic structure approaches to transition-metal catalysis. Quantum mechanical calculations can probe subtle mechanistic insights and thereby complement experimental information. Therefore, a thorough theoretical study on this reaction could qualitatively offer the simple concept needed to elucidate the manifold reactivity of the transition-metal oxide cations. Although the important ligand effects that often play an essential role in the reactivity of the transition-metal complex were not considered explicitly, the detailed electronic structure studies of this "simple" case can still be especially useful in interpreting the reaction profiles and understanding the reactivity and selectivity of these systems, and a thorough study on this fundamental reaction can provide important clues on the behavior of larger condensed-phased metal−oxo systems. In addition, the reactions of C−H bond activation by $[FeO]^{n+}$ cations with and without various ligands are also under investigation in our group.[89] We would like to systematically explain from a computational perspective how the reactivity changes as a function of different ligands coordinated to the iron center.

2. COMPUTATIONAL METHODS

Electronic structure calculations were mainly performed with the ORCA[90] package developed by the Neese group, Bonn University. For geometry optimizations, the hybrid B3LYP density functional[91−93] in combination with the triple-ζ quality TZVP basis set was employed throughout the study, as suggested by Shaik.[94] The RIJCOSX approximation was used to accelerate the calculations using the auxiliary basis set TZV/J at insignificant extra accuracy. All of the geometries were fully optimized without symmetry constraints using an open-shell formalism under vacuum conditions. Harmonic vibrational frequencies were computed to verify the nature of the stationary points. The minimum structures reported in this work possess only positive eigenvalues of the Hessian matrix, whereas the transition states (TSs) have only one negative eigenvalue. To corroborate the minima linked by the considered transition states, intrinsic reaction coordinate (IRC) calculations were also performed by the Gaussian 03 program.[95] The zero-point energies, thermal corrections, and entropy terms for the optimized geometries were obtained from frequency calculations. Although several methods to locate the minimum-energy crossing points (MECPs) do exist,[96] spin inversion point locations are only estimated on the basis of the IRC paths at the B3LYP level in the present study. To explore the probability of the spin-forbidden transition, spin−orbit coupling (SOC) matrix elements were calculated between the quartet and sextet states through quasi-degenerate perturbation theory at the SA-CASSCF/def2-TZVPP level with ORCA for the four located MECPs.[97] The CASSCF wave function of the title system contains active spaces of all of the unpaired

dx.doi.org/10.1021/jp2120302 | J. Phys. Chem. A 2012, 116, 1475−1485

Table 1. Calculated Gibbs Free-Energy[a] Using ^{6}R_d as the Reference Species

entry	$\Delta G_{(g)}$	$\Delta G_{(\varepsilon)}$	$\Delta G_{(s)}$	$\Delta G_{(CCSD(T))}$	entry	$\Delta G_{(g)}$	$\Delta G_{(\varepsilon)}$	$\Delta G_{(s)}$	$\Delta G_{(CCSD(T))}$
^{6}R_d	0.00	0.00	0.00	0.00	^{4}R_d	4.85	6.12	7.84	9.17
^{6}TSH_d	23.23	22.13	21.20	34.13	^{4}TSH_d	21.09	21.36	22.34	30.01
^{6}IM_d	−0.05	4.46	6.32	11.33	^{4}IM_d	1.39	3.92	5.76	11.53
^{6}TSRe_d	4.42	9.21	11.80	15.73	^{4}TSRe_d	9.34	13.32	15.72	22.08
^{6}P_nol	−25.72	−18.78	−13.88	−31.91	^{4}P_nol	−33.66	−26.66	−21.69	−29.91
^{6}R_c	0.24	0.11	1.01	4.38	^{4}R_c	3.09	4.72	6.82	6.69
^{6}IM_c	−23.71	−18.57	−14.64	−17.85	^{4}IM_c	−33.34	−29.46	−26.07	−11.48
^{6}IM_ene	−10.56	−4.92	−0.53	−5.36	^{4}IM_ene	−18.40	−13.40	−8.62	2.54
^{6}TSH_c5	21.86	21.61	22.91	29.29	^{4}TSH_c5	19.39	19.97	21.29	29.16
^{6}TSRe_nol	2.18	8.92	13.74	17.41	^{4}TSH_c4	17.71	18.95	20.78	23.67
^{6}TS_ene	0.82	6.38	10.51	3.85	^{4}TSRe_nol	0.66	5.35	9.14	15.12
^{6}TS1_ene	1.40	6.45	10.47	8.66	^{4}TS1_ene	−17.45	−13.06	−7.87	7.12
^{6}TS2_ene	11.56	17.00	21.14	14.85	^{4}TS2_ene	−13.48	−7.97	−3.67	−3.41
^{6}P_ene	−23.60	−17.09	−12.38	−29.53	^{4}TS_ene	−6.26	−1.36	2.32	6.98
					^{4}P_ene	−61.96	−56.01	−51.60	−41.05

[a] $\Delta G_{(g)}$, $\Delta G_{(\varepsilon)}$, and $\Delta G_{(s)}$ are relative B3LYP Gibbs free energies in the gas phase, with dielectric constant ε = 4 and acetonitrile (ε = 36.6) solvent conditions. $\Delta G_{(CCSD(T))}$ are relative Gibbs free energies in the gas phase at the CCSD(T) level of theory using B3LYP geometries. Units: kcal/mol.

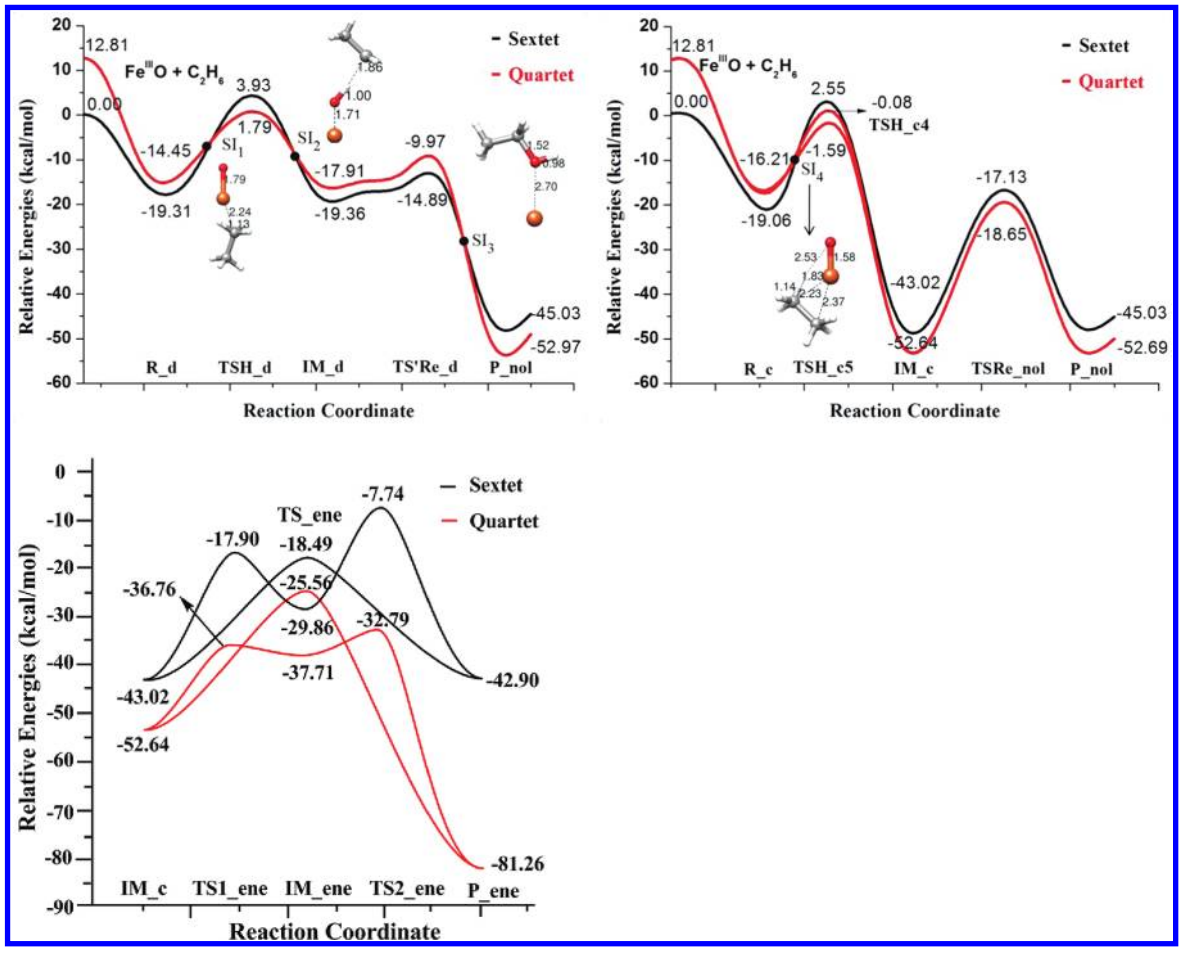

Figure 1. Schematic gas-phase Gibbs free-energy surfaces (ΔG) of ethane hydroxylation in the title reaction at the B3LYP level of theory in units of kcal/mol. (Top left) The direct H-abstraction mechanism. (Top right) The alcohol generation of the concerted H-abstraction mechanism along the reaction coordinates. (Bottom) The ethene generation of the concerted H-abstraction mechanism along the reaction coordinates. Spin inversion points are also shown.

electrons in their corresponding orbitals.[98] The SOC-induced quartet−sextet interaction can be expressed by root-mean-square coupling constant SOC = $[\sum \langle H \rangle^2]^{1/2}$ as proposed by Yoshizawa.[76]

Final energy refinement, that is, single-point energy (SPE), calculations were first performed with the hybrid B3LYP density functional using the new default basis sets of triple-ζ quality including high angular momentum polarization

dx.doi.org/10.1021/jp2120302 | J. Phys. Chem. A 2012, 116, 1475−1485

functions def2-TZVPP for all elements.[99] Coupled cluster theory CCSD(T) calculations for all reaction processes were also employed at the previous B3LYP geometries using def2-TZVP basis sets. The T1 magnitudes, often taken as a diagnostic measure of multireference character, lie well within the range of 0.007−0.036, which indicates reliable CCSD(T) results. Both of these SPE calculations were in gas-phase conditions. To take into account the role of solvent effects, the conductor-like screen model (COSMO) was also used. Acetonitrile was chosen as the solvent to mimic experimental conditions, and dielectric constant $\varepsilon = 4$ was chosen to mimic the protein environments, as suggested by Siegbahn.[31,100] All SPE calculations were accelerated by using the density fitting and chain of sphere (RIJCOSX) approximation.

The quasi-restricted molecular orbital (QRO)[101] of special points along the minimum-energy pathway (MEP) was calculated and plotted using Chimera.[102]

3. RESULTS AND DISCUSSIONS

Due to the several accessible spin states for the metal-containing active site, the reaction of ethane with FeO^+ has been explored on both the quartet spin (intermediate spin, IS) and sextet spin (high spin, HS) states. As found in the reaction of methane with FeO^+,[77] three different reaction pathways of the first H-atom abstraction have been examined, (1) direct H-abstraction, (2) five-centered H-abstraction, and (3) four-centered H-abstraction (Scheme 2). The first pathway is a typical direct H-abstraction mechanism, and the latter two pathways belong to a concerted mechanism. First, the direct H-abstraction is characterized by a collinear transition state C···H···O−Fe, which only involves the C−H bond breaking and O−H bond formation. Second, the concerted mechanism, just as its name implies, is featured by some bonds breaking and forming in a single step. In the current case, the C−H bond breaking and O−H bond formation are concomitant with a new Fe−C bond forming subsequently. The five-centered transition state finally leads to either ethanol or ethane products. Third, there is a second concerted reaction mechanism in which a four-centered transition state C···H···O−Fe is involved in its initial stages that then leads to the same intermediate as that found in the first concerted mechanism. The optimized geometries with selective parameters of the reactant complexes, transition states, intermediates, and products are plotted as shown in Figure S1 (Supporting Information, SI). The relative Gibbs free energies for the direct and five- and four-centered H-abstraction are listed in Table 1 and plotted in Figure 1. To give a deep insight into the electronic transfer behaviors, the schematic frontier molecular orbital (FMO) diagrams for all pathways are demonstrated in Figures 2−4, and additional MO diagrams are also provided in Figures S2−S4 in the SI. As shown herein, the second step of the reaction is much more favored to produce ethene as that final production than ethanol, and a proton-coupled electron transfer (PCET)[103] is pronounced from the detailed electronic structure analysis. In the following sections, we are going to discuss the different reactivity of these two reaction mechanisms in detail.

3.1. $[FeO]^+$. First, the detailed discussion of $[FeO]^+$ electronic structures can provide valuable clues to understanding the reaction mechanism of the two spin-state surfaces that will be investigated below. The orbital occupation patterns can be expressed as $^4\Sigma[(\text{Fe-d}_{x^2-y^2})^2(\text{Fe-d}_{xy})^1\pi^*(\text{Fe-d}_{xz})^1\pi^*(\text{Fe-d}_{yz})^1\sigma^*(\text{Fe-d}_{z^2})^0\pi(\text{O-p}_x)^2\pi(\text{O-p}_y)^2\sigma(\text{O-p}_z)^2]$ for the quartet state and $^6\Delta[(\text{Fe-d}_{xy})^1\pi^*(\text{Fe-d}_{xz})^1\pi^*(\text{Fe-d}_{yz})^1(\text{Fe-d}_{x^2-y^2})^1\sigma^*(\text{Fe-d}_{z^2})^1\pi(\text{O-p}_x)^2\pi(\text{O-p}_y)^2\sigma(\text{O-p}_z)^2]$ for the sextet one.[71,104,105] B3LYP calculations predict the quartet species to be 12.81 kcal/mol higher in energy than the corresponding sextet one.[72−74,98,104,106] The orbital occupation pattern implies an $Fe-O_{oxo}$ bond order of 1.5 in the sextet spin (HS) state compared to 2 in the quartet state. The reduction in the bond order in the HS state results in a significant lengthening of the $Fe-O_{oxo}$ bond (1.64 Å in $^6(FeO)^+$ versus 1.56 Å in $^4(FeO)^+$). The lengthening of the Fe−O bond combined with the electronic distribution change demonstrates that the π-bonding MO in the quartet state has more O radical component than that of the sextet state. As we know, the entire C−H bond activation process consists of a preparatory stage and the actual H-atom abstraction that is accomplished by the highly electrophilic oxyl radical, and the interaction of the O-p orbital with the electron donor affords a pair of three-centered MOs (σ_{CHO} and σ^*_{CHO}).[1,12,40]

3.2. Direct H-Abstraction Mechanism. We first discuss the hydroxylation reactions by direct H-abstraction based on the DFT calculations. Figure S1 (SI) gives the stationary points along the HS and IS pathways, and Figure 1 shows the calculated Gibbs free energy surface diagram along the entire reaction coordinates in which both two spin states are considered. One can find that this mechanism is actually the same as the well-accepted rebound mechanism for the C−H bond activation by heme and nonheme iron-oxo catalysts.[48] The processes via $^{6/4}$TSH_d represent the pathways on the sextet and quartet surfaces. It should be noted here that direct H-abstraction for the quartet state does not exist in the FeO^+/CH_4 system.[77] As shown in Figure S1A (SI), a prereaction complex R_d, which corresponds to a weak coordination of ethane to the iron center, is initially formed at the starting point. The relative energy of this complex on IS is calculated to be 4.85 kcal/mol above that on the HS surface. Structurally, dramatic differences exist. As shown in Figure S1A (SI), a relatively short Fe−C bond and a much longer Fe═O bond are found in the quartet state, while the Fe═O bond in the sextet state makes no big difference over that in the separate $[FeO]^+$ and ethane molecules. Starting from the prereaction complex, although a horizontal attack of the ethane on the Fe═O moiety is encountered for both spin states,[77] pronounced differences still exist. As shown in Figure S1A (SI), a more significant bent Fe−O−H angle (91.7°) is predicted for the quartet state compared to that in the sextet state (117.7°). Reasonable explanation can be found in the electronic analysis next. Again, the nearly collinear C−H−O array is exhibited by both $^{6/4}$TSH_d. The C−H bonds that are going to be broken are calculated to be 1.16 and 1.17 Å, which is analogous to the normal C−H bond at 1.12 Å. The O−H bonds that are going to be formed are found to be 1.59 and 1.64 Å, which is far away from the normal H−O bond at 0.97 Å. The calculated O−H and C−H bonds that are going to be formed and broken are reasonable for both spin states. Additionally, no big changes were found in the Fe═O bond and the geometry parameters of the alkyl radical. To sum up, all of these geometry characteristics indicate reactant-like, very early transition states. Very similar intermediates $^{6/4}$IM_d were also found in these two spin states, that is, the newly formed iron-hydroxyl species weakly bound to the alkyl radical moiety that is ready for the rebound step. At the last step, the intermediates pass through the O-rebound steps in which the alkyl radical associates with the $O^\bullet$ radical of the Fe−O−H moiety and leads to the ethanol

dx.doi.org/10.1021/jp2120302 | J. Phys. Chem. A 2012, 116, 1475−1485

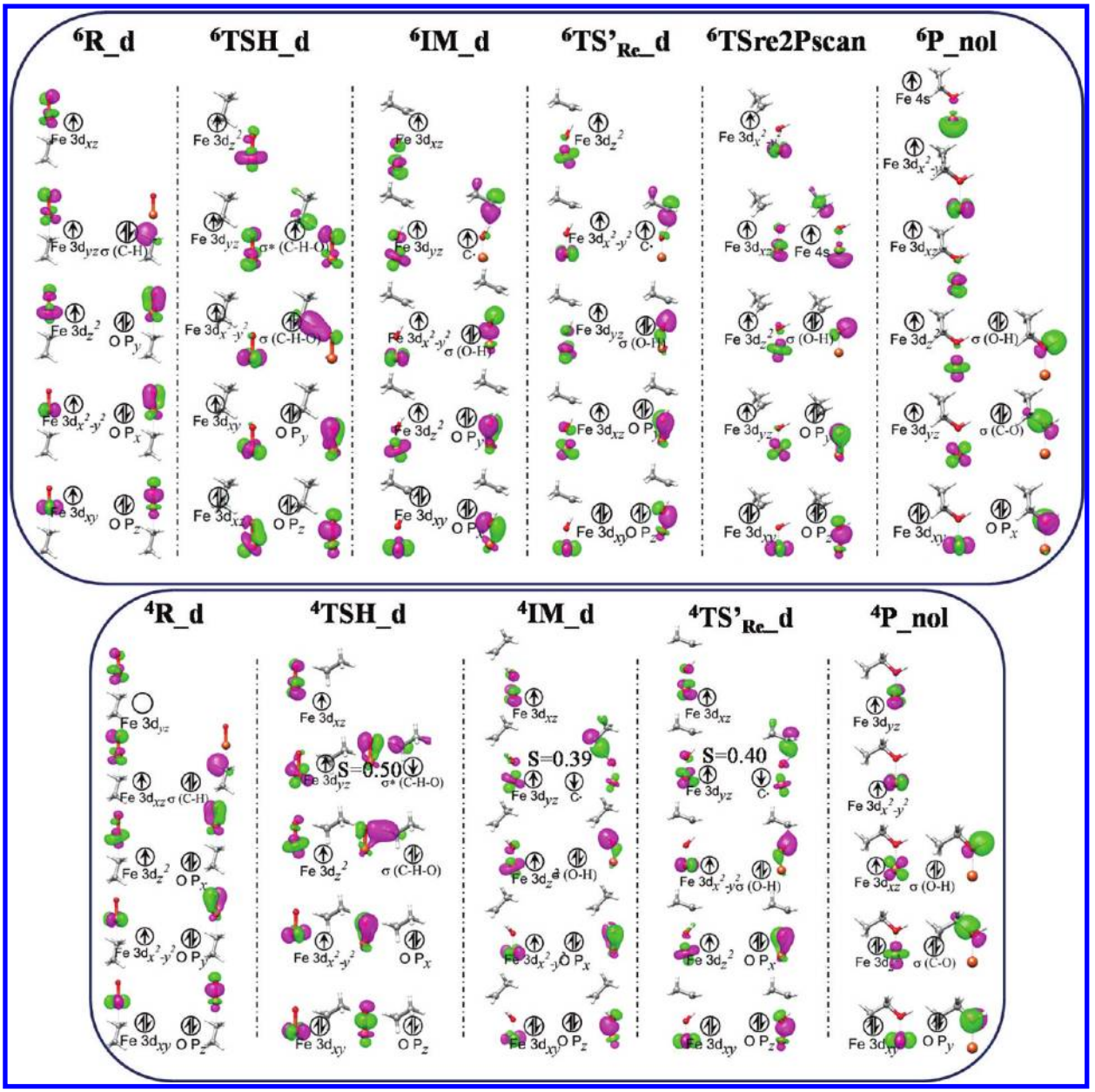

Figure 2. Schematic MO diagram of the sextet spin state and quartet ones along the reaction coordinates in the direct H-abstraction mechanism. (Top) sextet state; (bottom) quartet state. C, gray; Fe, orange; O, red.

product weakly bound to the Fe(I) ion. The structures ($^{6/4}$TS′$_{Re}$_d) shown in Figure S1A (SI) were captured from the maxima in the relaxed MEP scans. It should be mentioned here that although we were unable to located the suitable O-rebound[44,107] transition-state structures, the results from the relaxed MEP scans indicate that the processes possess considerable barriers of approximately 9.34 and 4.42 kcal/mol for the quartet and sextet states, respectively.

Now, let us inspect the electronic structure evolution during the whole process. Previous theoretical studies[33] demonstrated that the H-abstraction step on HS/IS surfaces can happen with either a σ-mechanism or π-mechanism, depending on the interaction of the σ_{C-H} bond with the O-based p_z orbital or the $p_{x/y}$ orbital. However, only one π-mechanism is established in this direct H-abstraction mechanism. The σ-mechanism is ruled out by the initially α-occupied Fe-based $3d_{z^2}$ orbital in the sextet state and the weak interaction between the substrate and iron center in the quartet state. As shown in Figure 2, the electronic structure of prereaction complex ^{6}R_d is best interpreted as a HS Fe(III) ion (S_{Fe} = 5/2) with five ferromagnetic α-electron spins. The five single α-spin-occupied Fe-based 3d orbitals make it impossible to accept a α-electron from the C−H σ-bond, which is commonly found in the established σ-mechanism. Therefore, the direct H-abstraction for the sextet state follows the nonclassical π-mechanism in which a β-electron shifts from the C−H σ-bond to the low-lying $\pi^*_{xz/yz}$ orbital. Spin density analyses are also consistent with the electronic structure discussed above. In ^{6}TSH_d, the spin density of the carbon atom that is going to lose a H atom is 0.21, which implicates the β-spin electron transfer during the C−H activation. This mechanism also offers a good explanation for the key geometry parameters, that is, the opposite requirements of optimal orbital overlap and Pauli repulsion lead to bent geometries ^{6}TSH_d with the Fe−O−H bent angle

dx.doi.org/10.1021/jp2120302 | J. Phys. Chem. A 2012, 116, 1475−1485

close to 120° (117.7°). Starting from ^{6}IM_d, the remaining α-electron of the alkyl radical is transferred to the Fe-based 4s orbital in the O-rebound step. One can find that five single α-electrons feature ferromagnetic spin on the Fe(I) ion (S_{Fe} = 5/2). In contrast to the sextet state in which the prereaction complex has essentially the same electronic structure as that in separate reactants, a different electronic structure of the prereaction complex ^{4}R_d is obtained. The weakly coordinated substrate to the iron center induced a much longer Fe═O bond and thereby greatly reduced the strong antibonding effect of $\sigma^*_{Fe=O}$. This can rationalize the electron occupation of the Fe $3d_z^2$ orbital in 4R_d. Now, the unoccupied $3d_{yz}$ orbital serves as the intrinsic electron-acceptor orbital, and the horizontal orientation of the orbital lobe attracts the substrate equatorially approaching the terminal oxo ligand.[37] It features the best orbital interactions and smallest Pauli repulsions and eventually leads to the bent geometry ^{4}TSH_d with a relatively small Fe−O−H angle close to 90° (91.7°). As shown in Figure 2, it becomes evident that the horizontal approaching of ethane toward the Fe−O moiety leads to an α-electron shift from the substrate to the unoccupied Fe-d_{yz} based orbital, resulting in the increase of spin polarization. Hence, the $3d_{yz}$ orbital should be the most potential electron acceptor; however, this pathway is different than the classically established π-mechanism. The intermediate ^{4}IM_d is characterized by the weakly antiferromagnetic coupling between an intermediate spin ferrous (S_{Fe} = 2) center and an alkyl radical (S_C = 1/2). Starting from ^{4}IM_d, the rebound step follows a σ-mechanism like that in the established quintet π-channel,[33] in which the remaining β-electron of the alkyl radical is transferred to the Fe-based $3d_{xz}$ orbital and leads to an Fe(I) ion (S_{Fe} = 3/2) .

After finishing the individual analyses for two spin states, we now turn to look at the big picture. As shown in Figure 1, B3LYP calculations show that the Gibbs free energies in the quartet and sextet states lie close and involve three crossing junctions that can provide a chance of spin-forbidden transition, which leads to a decrease in the barrier height corresponding to the hydrogen abstraction and O-rebound, respectively. In this work, we successfully located the three spin inversion points at the B3LYP level, and the SOC matrix elements between the sextet and quartet states are 315.6, 109.4, and 0 cm^{-1} for Figures SI_1, SI_2, and SI_3, respectively.[108] The strong strength of the SOC between the sextet and quartet states indicates a typical TSR scenario (Scheme 3).[73] The quartet Gibbs free-energy surface should therefore play an essential role in this reaction as it did in the methane and benzene hydroxylation by FeO^+ if a spin-forbidden transition between the two states takes place.[82,76,109] Like the radical mechanism for the direct methane-to-methanol and benzene-to-phenol conversions by the FeO^+ cation in which there is a spin crossing of two Gibbs free-energy surfaces,[76,109] the direct H-abstraction pathways may also start with sextet state reactants and then proceed on the energetically lower-lying quartet spin pathway in the HAT step; however, it should pass through the sextet state reaction pathway and end with the quartet state products in the following O-rebound step. Electronically, as we mentioned above, the direct H-abstraction mechanism will proceed with spin−flip after the initial prereaction complex ^{6}R_d and lead to crossing over of the two Gibbs free-energy surfaces. Figure 2 clearly shows the spin inversion of the alkyl radical. The notable effects of the spin inversion can be found in the two transition states of this mechanism. Therefore, spin−orbit coupling is large enough in the α-electron-occupied alkyl radical of the FeO^+/C_2H_6 system, TSR is primarily expected, and the quartet Gibbs free-energy surface should play an essential role in this direct H-abstraction reaction. As shown in Figure 1, the pathways of the sextet and quartet surfaces have comparable rate-controlling energy barriers $^{6/4}$TSH_d of 23.23 and 21.09 kcal/mol, respectively, indicating that the quartet state pathway could have slightly higher reactivity.

Scheme 3

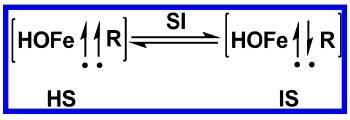

3.3. Concerted H-Abstraction. Figure S1B (SI) shows optimized geometries of the reaction intermediates and the transition states, and Figure 1 shows the Gibbs free-energy profiles for the HS and IS reaction pathways in the concerted H-abstraction. As found in the direct H-abstraction mechanism, the reaction pathways of the concerted H-abstraction mechanism also initially proceed via a prereaction complex, which is formed through the electrostatic interactions between FeO^+ and ethane, $[OFe\cdots C_2H_6]^+$. Actually, they are essentially the same as those found in the direct H-abstraction mechanism. By comparison the Gibbs free-energy surfaces and all of the geometry structures, the differences between the two reaction mechanisms can be ascribed to three aspects. First, the H-abstraction process in the concerted mechanism proceeds through a five- or four-centered transition state. The five/four-centered cyclic structures make the C−H−O angle slightly deviate from the collinear arrangement in the direct H-abstraction mechanism. As shown in Figure S1 B (SI), the calculated C−H−O angles are 91.9°/106.3° for ^{6}TSH_c5 and ^{4}TSH_c5, respectively. For the five-centered transition states, the optimized geometry structures demonstrate a relatively tighter five-centered ring in ^{6}TSH_c5 than that in ^{4}TSH_c5, which indicates a much earlier transition state encountered by the quartet state. The four-centered transition state ^{4}TSH_c4 is only located on the quartet state, and it is energetically close to the quartet state five-centered one. Second, in contrast to the intermediates $^{6/4}$IM_d in the direct H-abstraction mechanism in which the alkyl radical is weakly bound to the hydroxyl ligand, the alkyl radicals in $^{6/4}$IM_c are weakly coupled to the iron center. As presented in Figure S1B (SI), after the H-abstraction by the terminal oxo, the five-centered cyclic structures are entirely broken, leading to the total separation of the alkyl radical and hydroxyl group ($^{6/4}$IM_c). Third, two different products, alcohol and ethene, are produced in this reaction mechanism. The nonclassical O-rebound step through $^{6/4}TS_{Re}$_nol yields the same hydroxylation products as those found in the direct H-abstraction mechanism. The ethene products can be generated via two different reaction pathways. A stepwise process that goes through two three-centered H-shift transition states $^{6/4}$TS1_ene and $^{6/4}$TS2_ene is the first potential one, and it has been established elsewhere.[88] The second possible pathway is first established in the current research and characterized by a "H" transfer via similar five-centered transition states $^{6/4}$TS_ene. The salient feature of the first pathway is that the iron metal is the reactive center, that is, the second H atom undergoes the migration through Fe to the hydroxyl ligand, while the second one is better described as a PCET, vide infra.[8,110−112]

dx.doi.org/10.1021/jp2120302 | J. Phys. Chem. A 2012, 116, 1475−1485

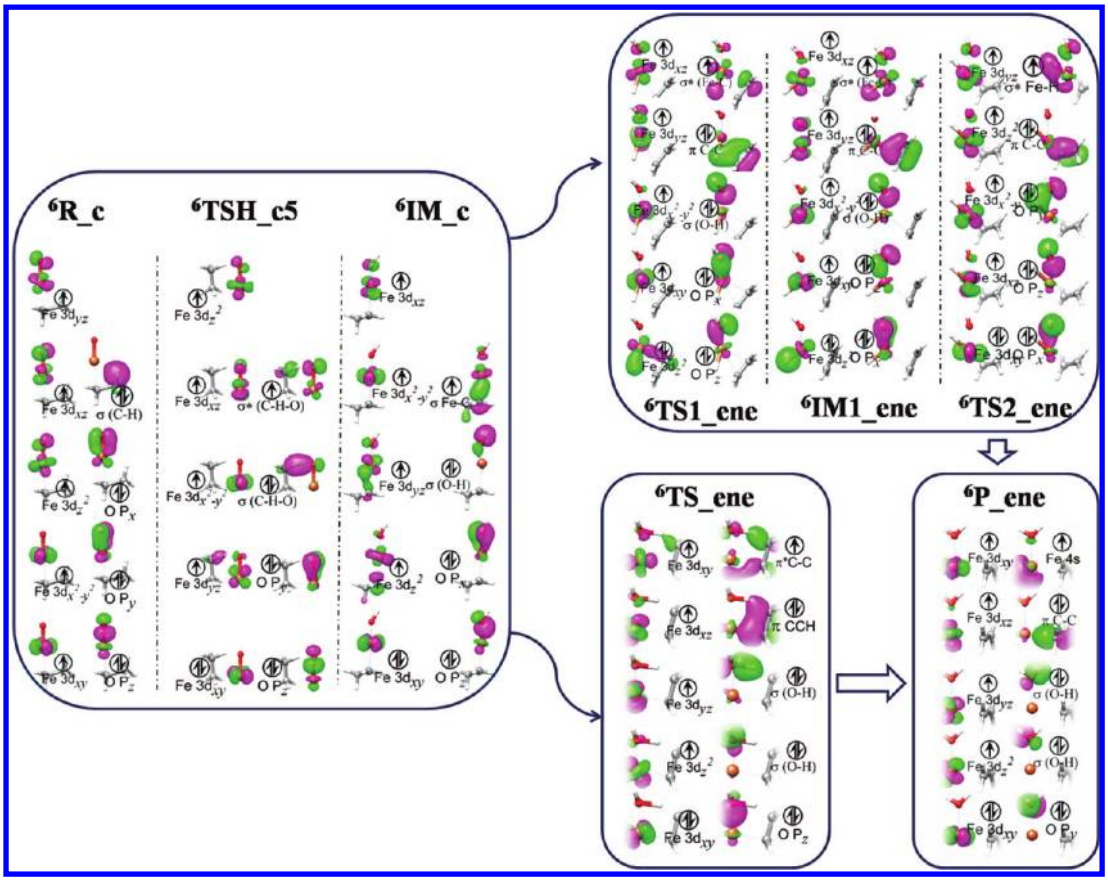

Figure 3. Schematic MO diagram of the sextet spin state along the reaction coordinates in the concerted H-abstraction mechanism. C, gray; Fe, orange; O, red.

For the entire reaction, the calculated Gibbs free-energy surface also suggests a two-state reactivity where the reaction starts on the HS surface and then comes across to the energetically lower-lying IS to finish the H-abstraction and all of the subsequent steps favorably. First, the slight energetic superiority of ^{4}TSH_c4 over ^{4}TSH_c5 makes the first H-abstraction process mainly through the four-centered transition state. The strength of the SOC matrix elements (300.6 cm^{-1}) of SI_4 indicates the ease of the spin-forbidden transition probability. This is also fully consistent with the results proposed by Yoshizawa and co-workers that the four-centered H-abstraction plays a central role in the gas-phase reaction between FeO^+ and methane. Then, the much lower energy barriers for the ethene conversion processes compared to those for ethanol conversion indicate a large productivity of ethene. Again, this is in good agreement with the experimental results that ethene is the major product of the reaction of FeO^+ with ethane.[69] It should be emphasized here that the mixed reactivity of oxidation−dehydrogenation was also proposed by Visser and Shaik.[57,58] The calculated energy barriers for these two pathways are close to each other, 26.08 and 15.89/18.86 kcal/mol (relative to ^{4}IM_c) for the five-centered transition state ^{4}TS_ene and the stepwise process at the B3LYP(gas) level of theory, respectively. The pathway through ^{4}TS2_ene has relatively lower-energy barrier ($\Delta\Delta G$ > 7 kcal/mol), the stepwise character seems more effective to reach the final products, and the process through the single five-centered transition state should have less competition. However, the relative competitive behavior reverses at the CCSD(T)//B3LYP levels of theory, which indicates that the one-step pathway may be the dominant process to the final product.

Detailed electronic structure analysis may provide key clues for interpreting the different reactive behaviors of quartet and sextet state surfaces. Figures 3 and 4 demonstrate the schematic FMO of the critical points along the sextet and quartet state reaction pathways in the concerted H-abstraction mechanism, and detailed MO information for the minor pathways is deposited as SI. The electron-transfer pathways of the first H-abstraction for the pathways via four- and five-centered ring transition states in Figures 3 and 4 are essentially the same as those found in the corresponding direct H-abstraction mechanism, that is, a β-electron from the substrate shifted to the Fe-based 3d orbital found in both the sextet state and the quartet state involves a α-electron shift to the iron center. The big differences between the two reaction mechanisms start from the intermediates $^{6/4}$IM_c. The alkyl radical in $^{6/4}$IM_c is bound to the iron center via a ligand−metal σ-bond, in contrast to the weak coupled effect for the hydroxyl ligand in $^{6/4}$IM_d (Figures S4 and S5, SI). The weak ferromagnetic coupling between the alkyl radical and the iron center in ^{6}IM_c is in good agreement with the geometry structure in which a relatively longer Fe−C bond is formed, while the short Fe−C bond in ^{4}IM_c is well-rationalized by the strong antiferromagnetic effect between the two moieties. The large orbital overlap value of 0.90 between Fe d_{z^2} and the C radical in ^{4}IM_c also confirms our analysis.

Starting from $^{6/4}$IM_c, the electron-transfer pathways for the hydroxylation product are again the same as those in the direct H-abstraction mechanism (SI). Therefore, we only focus on the

dx.doi.org/10.1021/jp2120302 | J. Phys. Chem. A 2012, 116, 1475−1485

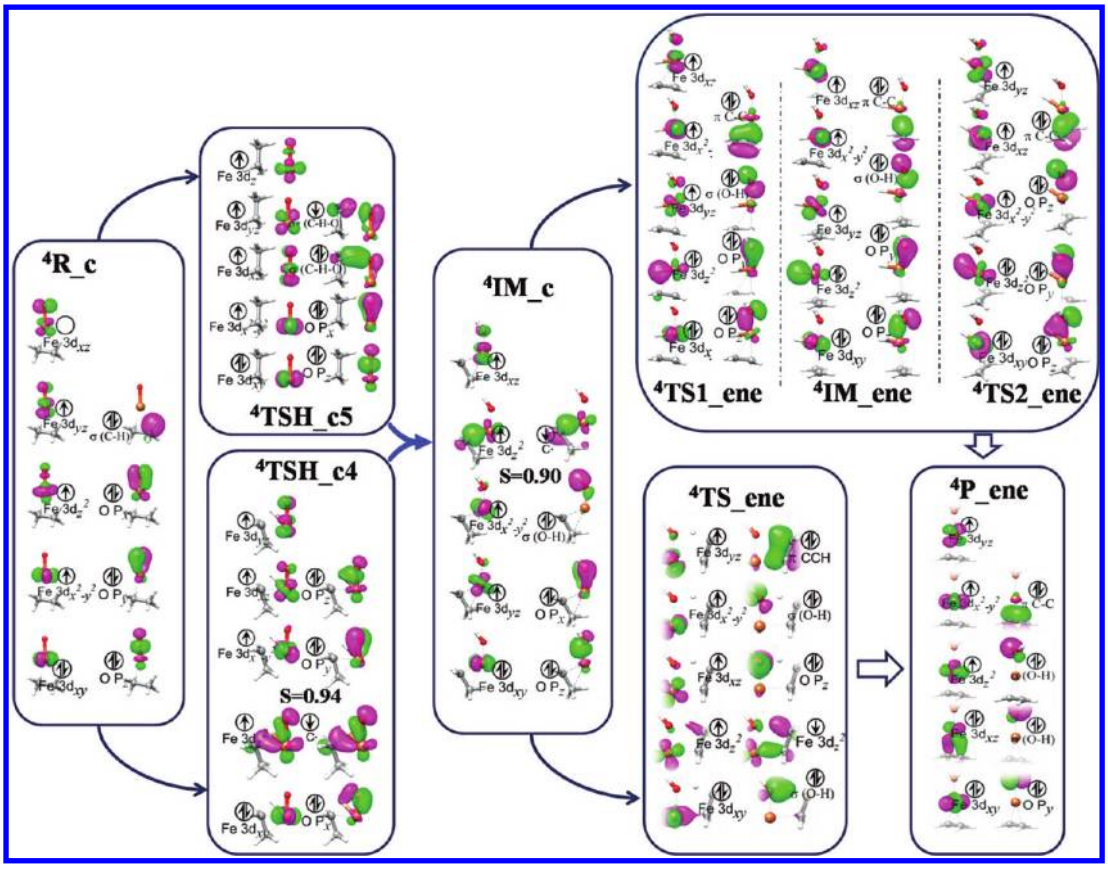

Figure 4. Schematic MO diagram of the quartet spin state along the reaction coordinates in the concerted H-abstraction mechanism. C, gray; Fe, orange; O, red.

electron evolution for the pathways leading to the ethene product in the following discussion. The electronic evolution for the well-established stepwise process first goes through a HAT to the iron center and then follows a proton transfer to the hydroxyl ligand, leading to the water and ethene weakly bound to the lone iron. As shown in Figure 3, in the sextet state, the proton from the methyl terminal migrates to the iron center, and at the same time, the electron in the α-occupied σ_{Fe-C} bond is redistributed to the Fe-based 4s orbital with an antibonding σ^*_{Fe-C}. The residual lone-pair electrons on the alkyl form a $\pi_{C=C}$ double bond in ^{6}IM_ene, while in the quartet state, as shown in Figure 4, the hydrogen atom shifted to the iron center is from the methyl terminal, and during this process, it is one β-electron in the σ_{C-H} of the alkyl radical transferred to Fe. Together with the existing α-electron on Fe, the Fe-based $3d_{z^2}$ orbital becomes doubly occupied, and the residual α-electron on the alkyl coupling with the other β-electron results in a $\pi_{C=C}$ double bond. Subsequently, a proton starting from the iron center transfers to the hydroxyl moiety with generation of ethene and a water molecule weakly coupled to the Fe(I) cation in both the HS and IS state pathways.

As for the one-step H transfer process via the five-centered transition state ^{6}TS_ene, it is a pronounced (PCET process. As shown in Figure 4, it starts with a proton transfer from the C atom of the methyl array to the O atom of the hydroxyl group. Concertedly, an α-electron from the other C atom of the CH_2 terminal is directly shifted to the Fe-based 4s orbital, leading to the final H_2O and ethene products weakly bound to the Fe(I) center. Clearly, two different transfer pathways are established for the proton and electron transfer, which is the same as that defined by PCET.[103,113] A similar electronic transfer pattern is proposed for the IS state. It is also via a PCET mechanism that the proton from the methyl array is shifted to the hydroxyl group while a β-electron, rather than an α-electron, is transferred from the CH_2 part directly to the iron center.

3.4. Reactivity and Energies. To compare the reactivity of the different mechanisms and different reaction conditions for the ethane C−H bond activation by Fe═O$^+$, we recalculated the whole Gibbs free-energy surface under gas-phase, acetonitrile (ε = 36.6) and with dielectric constant ε = 4 conditions at the B3LYP/def2-TZVPP level. We also performed the energy refinement calculations under the CCSD(T) level to confirm our DFT calculations, as listed in Table 1. First, at the B3LYP-gas level, the concerted mechanism through TSH_c5 is the most feasible reaction pathway. As show in Table 1, although the precomplex ^{6}R_d in the direct H-abstraction is the most stable species, the relatively higher energy barrier of quartet TSH_d compared to that of the quartet TSH_c5 in the concerted H-abstraction, together with the spin-forbidden transition allowance, clearly indicates that the concert mechanism is favorable. Second are the solvent effects. As listed in Table 1, one can find that the relative energies of the stationary points along the pathways lie higher and become more unstable under larger dielectric constant conditions except for the ^{6}TSH_d. This effect becomes sharp from the reactant side to the product except for the quartet reactants. As Baerends proposed that the smaller screening effect of solvents led to the lower barrier for the H-abstraction by Fe^{IV}═O,[45] our implicit solvent results show that the Fe═O$^+$ reactivity become sluggish when changing from the gas

dx.doi.org/10.1021/jp2120302 | J. Phys. Chem. A 2012, 116, 1475−1485

phase to polar solution. Third is the total formal charge influence. Usually, the formal charge of the electrophilic agents has dramatic influence on the energies of electron-accepting orbitals (EAOs). The higher the formal charge of the oxidant, the lower the energy of EAO, and a more powerful electrophile for the C−H bond activation is therefore expected. In the current study (Fe^{III}=O^{+}), the most favorable pathway is calculated to be 17.47 and >20 kcal/mol in vacuum and acetonitrile conditions, respectively, much higher than that (about 10 kcal/mol) of ethane C−H bond activation by $[Fe^{IV}(O)(NH_3)_5]^{2+}$.[33] This is in good agreement with the argument proposed by Thiel and de Visser et al. that the higher oxidized species are more reactive toward C−H bond hydroxylation.[30,43]

The CCSD(T) level energies based on B3LYP optimized geometries predict slightly larger energy barriers for all of the pathways leading to the ethanol product, as shown in Table 1. For the ethene product, the same behavior is also found on the quartet state surface. However, much lower energies are obtained for the sextet state case. This may be attributed to the slight bias of the high-spin state of the CCSD(T) results because all of these pathways involve late transition states that possess a high-spin Fe(I) (S_{Fe} = 5/2) center.[33] In particular, another point that we must emphasize here is that CCSD(T) results give a relatively lower energy barrier for the one-step process to the ethene product compared to the stepwise one. Therefore, the newly established one-step PCET pathway may be the dominant process leading to the final product. However, close inspection of the energies predicted by B3LYP and CCSD(T) methods shows that the B3LYP functional seems to underestimate the energy barriers in both quartet and sextet spin state surfaces. This is in good agreement with the very recent research by Shaik in which they calibrated many density functional results with high-level ab initio coupled cluster methods and suggested the use of B3LYP in theoretical studies where reactivity comparison between different spin state is important and can be recommended.[94]

4. CONCLUSION

In this study, the direct oxidation of ethane to products ethanol and ethene by the bare Fe^{III}=O^{+} cation have been explored extensively. The detailed geometry and energetic and electronic structural analyses are presented. Two possible reaction mechanisms are available in the entire reaction, that is, the direct H-abstraction mechanism and the concerted mechanism. In the direct H-abstraction mechanism, a direct H-abstraction is encountered in the initial step, going through a collinear transition state C···H···O−Fe TSH_d, and results in an intermediate Fe−OH weakly bonded to an alkyl radical species. The final product of this mechanism is ethanol, which is produced by the hydroxyl group rebound to the carbon radical. In the concerted reaction mechanism, the H-abstraction process is characterized by overcoming the four/five-centered transition states $^{6/4}$TSH_c5 or ^{4}TSH_c4. The second step of the concerted mechanism can lead to either ethanol or ethene. Moreover, the major product ethene can be generated through two different pathways, the one-step pathway and the stepwise one. We must stress here that it is the first report where the one-step pathway starting from $^{6/4}$IM_c to product can be better described as a proton-coupled electron transfer (PCET).[114−119] It plays an important role in the product ethene generation according to the CCSD(T) results. The inherent factors of electron transfer are also discussed. The Gibbs free-energy surfaces and SOC matrix elements of spin inversion points demonstrate that the title reaction should follow the two-state reactivity (TSR) pattern that the spin-forbidden transition could slightly lower the energy barrier. The thorough theoretical study, especially the electronic structure analysis, may provide important clues for understanding and studying the C−H bond activation promoted by iron-based artificial catalysts.

■ ASSOCIATED CONTENT

Supporting Information

The evolution of frontier molecular orbitals (FMO) of the sextet and quartet state $[Fe^{III}O]^{+}$ as a function of Fe−O bond distance, the evolution of FMO of sextet and quartet states along the reaction coordinates, the optimized geometries of the reactant complexes, transition states, intermediates and products, and the values of T1 dignostics in CCSD(T) calculations. This material is available free of charge via the Internet at http://pubs.acs.org.

■ AUTHOR INFORMATION

Corresponding Author

*E-mail: jilai@jlu.edu.cn. Fax: (+)86-431-88499721.

Notes

The authors declare no competing financial interest.

■ ACKNOWLEDGMENTS

This work is supported by the National Natural Science Foundation of China (NSFC No. 21103064, 21073075, 21173097), the Research Fund for the Doctoral Program of Higher Education of China (RFDP No. 20100061110046), the Special Funding of the State Key Laboratory of Theoretical and Computational Chemistry, Jilin University, and the Basic Research Fund of Jilin University (No. 421010061439, 450060445067). The authors are indebted to Dr. D. Ganyushin, Max−Planck Institute for Bioinorganic Chemistry, Mülheim an der Ruhr, Germany, for discussion on SOC.

■ REFERENCES

(1) Ogliaro, F.; Harris, N.; Cohen, S.; Filatov, M.; de Visser, S. P.; Shaik, S. *J. Am. Chem. Soc.* **2000**, *122*, 8977.
(2) Ortiz de Montellano, P. R. *Chem. Rev.* **2010**, *110*, 932.
(3) Kamachi, T.; Yoshizawa, K. *J. Am. Chem. Soc.* **2003**, *125*, 4652.
(4) Shaik, S.; Cohen, S.; Wang, Y.; Chen, H.; Kumar, D.; Thiel, W. *Chem. Rev.* **2009**, *110*, 949.
(5) Green, M. T. *Curr. Opin. Chem. Biol.* **2009**, *13*, 84.
(6) Ortiz de Montellano, P. R. *Drug Metab. Rev.* **2008**, *40*, 405.
(7) Shaik, S.; Kumar, D.; de Visser, S. P.; Altun, A.; Thiel, W. *Chem. Rev.* **2005**, *105*, 2279.
(8) Meunier, B.; de Visser, S. P.; Shaik, S. *Chem. Rev.* **2004**, *104*, 3947.
(9) Green, M. T.; Dawson, J. H.; Gray, H. B. *Science* **2004**, *304*, 1653.
(10) de Montellano, P. R. O.; Nelson, S. D. *Arch. Biochem. Biophys.* **2011**, *507*, 95.
(11) Cooper, H. L. R.; Groves, J. T. *Arch. Biochem. Biophys.* **2011**, *507*, 111.
(12) Shaik, S.; Lai, W.; Chen, H.; Wang, Y. *Acc. Chem. Res.* **2010**, *43*, 1154.
(13) Hirao, H.; Kumar, D.; Thiel, W.; Shaik, S. *J. Am. Chem. Soc.* **2005**, *127*, 13007.
(14) Schöneboom, J. C.; Cohen, S.; Lin, H.; Shaik, S.; Thiel, W. *J. Am. Chem. Soc.* **2004**, *126*, 4017.
(15) Lai, W.; Shaik, S. *J. Am. Chem. Soc.* **2011**, *133*, 5444.
(16) de Visser, S. P.; Shaik, S. *J. Am. Chem. Soc.* **2003**, *125*, 7413.

(17) Usharani, D.; Janardanan, D.; Shaik, S. *J. Am. Chem. Soc.* **2011**, *133*, 176.
(18) Shaik, S.; Kumar, D.; de Visser, S. P. *J. Am. Chem. Soc.* **2008**, *130*, 10128.
(19) Groves, J. T.; Shaik, S.; Ogliaro, F.; De Visser, S. P. *Angew. Chem., Int. Ed.* **2001**, *40*, 3503.
(20) Decker, A.; Rohde, J.-U.; Klinker, E. J.; Wong, S. D.; Que, L.; Solomon, E. I. *J. Am. Chem. Soc.* **2007**, *129*, 15983.
(21) Wong, S. D.; Bell, C. B. III; Liu, L. V.; Kwak, Y.; England, J.; Alp, E. E.; Zhao, J.; Que, L. Jr.; Solomon, E. I. *Angew. Chem., Int. Ed.* **2011**, *50*, 3215.
(22) Solomon, E. I.; Wong, S. D.; Liu, L. V.; Decker, A.; Chow, M. S. *Curr. Opin. Chem. Biol.* **2009**, *13*, 99.
(23) Dey, A.; Jiang, Y.; de Montellano, P. O.; Hodgson, K. O.; Hedman, B.; Solomon, E. I. *J. Am. Chem. Soc.* **2009**, *131*, 7869.
(24) Li, F.; Meier, K. K.; Cranswick, M. A.; Chakrabarti, M.; Van Heuvelen, K. M.; Muenck, E.; Que, L. Jr. *J. Am. Chem. Soc.* **2011**, *133*, 7256.
(25) Hirao, H.; Li, F.; Que, L. Jr.; Morokuma, K. *Inorg. Chem.* **2011**, *50*, 6637.
(26) Benighaus, T.; Thiel, W. *J. Comput. Chem.* **2009**, *5*, 3114.
(27) Benighaus, T.; Thiel, W. *J. Comput. Chem.* **2011**, *7*, 238.
(28) Metz, S.; Thiel, W. *J. Am. Chem. Soc.* **2009**, *131*, 14885.
(29) Wang, D. Q.; Thiel, W. *J. Mol. Struct: THEOCHEM* **2009**, *898*, 90.
(30) Altun, A.; Shaik, S.; Thiel, W. *J. Am. Chem. Soc.* **2007**, *129*, 8978.
(31) Siegbahn, P. E. M.; Borowski, T. *Faraday Discuss.* **2011**, *148*, 109.
(32) Siegbahn, P. E. M.; Borowski, T. *Acc. Chem. Res.* **2006**, *39*, 729.
(33) Geng, C. Y.; Ye, S. F.; Neese, F. *Angew. Chem., Int. Ed.* **2010**, *49*, 5717.
(34) Ye, S. F.; Neese, F. *Proc. Natl. Acad. Sci. U.S.A.* **2011**, *108*, 1228.
(35) Ye, S.; Neese, F. *Curr. Opin. Chem. Biol.* **2009**, *13*, 89.
(36) de Visser, S. P. *J. Am. Chem. Soc.* **2006**, *128*, 9813.
(37) de Visser, S. P. *J. Am. Chem. Soc.* **2006**, *128*, 15809.
(38) de Visser, S. P.; Kumar, D.; Cohen, S.; Shacham, R.; Shaik, S. *J. Am. Chem. Soc.* **2004**, *126*, 8362.
(39) de Visser, S. P.; Ogliaro, F.; Sharma, P. K.; Shaik, S. *J. Am. Chem. Soc.* **2002**, *124*, 11809.
(40) de Visser, S. P.; Ogliaro, F.; Harris, N.; Shaik, S. *J. Am. Chem. Soc.* **2001**, *123*, 3037.
(41) de Visser, S. P. *J. Am. Chem. Soc.* **2010**, *132*, 1087.
(42) de Visser, S. P.; Kumar, D.; Cohen, S.; Shacham, R.; Shaik, S. *J. Am. Chem. Soc.* **2004**, *126*, 8362.
(43) Tahsini, L.; Bagherzadeh, M.; Nam, W.; de Visser, S. P. *Inorg. Chem.* **2009**, *48*, 6661.
(44) Michel, C.; Baerends, E. J. *Inorg. Chem.* **2009**, *48*, 3628.
(45) Ensing, B.; Buda, F.; Gribnau, M. C. M.; Baerends, E. J. *J. Am. Chem. Soc.* **2004**, *126*, 4355.
(46) Shaik, S.; de Visser, S. P.; Ogliaro, F.; Schwarz, H.; Schröder, D. *Curr. Opin. Chem. Biol.* **2002**, *6*, 556.
(47) Schwarz, H.; Beerhues, L. *Arch. Pharm. (Weinheim, Ger.)* **2001**, *334*, 10.
(48) Groves, J. T.; McClusky, G. A. *J. Am. Chem. Soc.* **1976**, *98*, 859.
(49) Su, J.; Groves, J. T. *J. Am. Chem. Soc.* **2009**, *131*, 12979.
(50) Filatov, M.; Harris, N.; Shaik, S. *Angew. Chem., Int. Ed.* **1999**, *38*, 3510.
(51) Schoneboom, J. C.; Lin, H.; Reuter, N.; Thiel, W.; Cohen, S.; Ogliaro, F.; Shaik, S. *J. Am. Chem. Soc.* **2002**, *124*, 8142.
(52) Ogliaro, F.; de Visser, S. P.; Cohen, S.; Sharma, P. K.; Shaik, S. *J. Am. Chem. Soc.* **2002**, *124*, 2806.
(53) Sun, X. L.; Li, J. L.; Huang, X. R.; Sun, C. C. *Curr. Inorg. Chem.* **2012**, *2*, 64.
(54) Pitie, M.; Pratviel, G. *Chem. Rev.* **2010**, *110*, 1018.
(55) Gunay, A.; Theopold, K. H. *Chem. Rev.* **2010**, *110*, 1060.
(56) Ener, M. E.; Lee, Y.-T.; Winkler, J. R.; Gray, H. B.; Cheruzel, L. *Proc. Natl. Acad. Sci. U.S.A.* **2010**, *107*, 18783.
(57) Kumar, D.; De Visser, S. P.; Shaik, S. *J. Am. Chem. Soc.* **2004**, *126*, 5072.
(58) Kumar, D.; Tahsini, L.; de Visser, S. P.; Kang, H. Y.; Kim, S. J.; Nam, W. *J. Phys. Chem. A* **2009**, *113*, 11713.
(59) Brönstrup, M.; Schröder, D.; Schwarz, H. *Chem.—Eur. J.* **2000**, *6*, 91.
(60) Schröder, D.; Schwarz, H. *Helv. Chim. Acta* **1992**, *75*, 1281.
(61) Schröder, D.; Schwarz, H. *ChemInform* **1992**, 23.
(62) Cho, K. B.; Shaik, S.; Nam, W. *Chem. Commun.* **2010**, *46*, 4511.
(63) Jackson, T. C.; Jacobson, D. B.; Freiser, B. S. *J. Am. Chem. Soc.* **1984**, *106*, 1252.
(64) Schröder, D.; Schwarz, H. *Angew. Chem., Int. Ed.* **1990**, *29*, 1433.
(65) Yoshizawa, K. *Acc. Chem. Res.* **2006**, *39*, 375.
(66) Yoshizawa, K.; Yumura, T. *J. Inorg. Biochem.* **2003**, *96*, 257.
(67) Yoshizawa, K. *J. Inorg. Biochem.* **1999**, *74*, 58.
(68) Yoshizawa, K.; Shiota, Y.; Yamabe, T. *Chem.—Eur. J.* **1997**, *3*, 1160.
(69) D. Schröder, H. S. *Angew. Chem., Int. Ed. Engl.* **1990**, *29*, 1433.
(70) Bohme, D. K.; Schwarz, H. *Angew. Chem., Int. Ed.* **2005**, *44*, 2336.
(71) Schröder, D.; Schwarz, H. *Angew. Chem., Int. Ed. Engl.* **1995**, *34*, 1973.
(72) Shaik, S.; Danovich, D.; Fiedler, A.; Schröder, D.; Schwarz, H. *Helv. Chim. Acta* **1995**, *78*, 1393.
(73) Schröder, D.; Shaik, S.; Schwarz, H. *Acc. Chem. Res.* **2000**, *33*, 139.
(74) Harris, N.; Shaik, S.; Schröder, D.; Schwarz, H. *Helv. Chim. Acta* **1999**, *82*, 1784.
(75) Yumura, T.; Yoshizawa, K. *Bull. Chem. Soc. Jpn.* **2004**, *77*, 1305.
(76) Shiota, Y.; Yoshizawa, K. *J. Chem. Phys.* **2003**, *118*, 5872.
(77) Yoshizawa, K. *Coord. Chem. Rev.* **2002**, *226*, 251.
(78) Yoshizawa, K. *J. Organomet. Chem.* **2001**, *635*, 100.
(79) Yoshizawa, K.; Kamachi, T.; Shiota, Y. *J. Am. Chem. Soc.* **2001**, *123*, 9806.
(80) Shiota, Y.; Yoshizawa, K. *J. Am. Chem. Soc.* **2000**, *122*, 12317.
(81) Yoshizawa, K.; Ohta, T.; Eda, M.; Yamabe, T. *Bull. Chem. Soc. Jpn.* **2000**, *73*, 401.
(82) Yoshizawa, K.; Shiota, Y.; Yumura, T.; Yamabe, T. *J. Phys. Chem. B* **2000**, *104*, 734.
(83) Yoshizawa, K.; Shiota, Y.; Kagawa, Y.; Yamabe, T. *J. Phys. Chem. A* **2000**, *104*, 2552.
(84) Yoshizawa, K.; Shiota, Y.; Kagawa, Y. *Bull. Chem. Soc. Jpn.* **2000**, *73*, 2669.
(85) Yoshizawa, K.; Shiota, Y.; Yamabe, T. *J. Phys. Chem.* **1999**, *111*, 538.
(86) Yoshizawa, K.; Suzuki, A.; Yamabe, T. *J. Am. Chem. Soc.* **1999**, *121*, 5266.
(87) Altinay, G.; Citir, M.; Metz, R. B. *J. Phys. Chem. A* **2010**, *114*, 5104.
(88) Zhao, L.; Guo, W.; Liu, Z.; Li, Y.; Lu, X. *Theor. Chim. Acta* **2011**, *128*, 349.
(89) Li, J. L.; Zhang, X.; Huang, X. R. *Phys. Chem. Chem. Phys.* **2012**, *14*, 246.
(90) Neese, F. *ORCA — An Ab Initio, Density Functional and Semiempirical Program Package 2010*, version 2.8; Bonn University: Germany, 2010.
(91) Becke, A. D. *J. Chem. Phys.* **1993**, *98*, 5648.
(92) Lee, C. T.; Yang, W. T.; Parr, R. G. *Phys. Rev. A* **1988**, *37*, 785.
(93) Schafer, A.; Huber, C.; Ahlrichs, R. *J. Chem. Phys.* **1994**, *100*, 5829.
(94) Chen, H.; Lai, W.; Shaik, S. *J. Phys. Chem. Lett.* **2010**, *1*, 1533.
(95) Frisch, M. J.; Trucks, G. W. S., H. B.; Scuseria, G. E.; Robb, M. A.; Cheeseman, J. R.; Montgomery, J. A., Jr.; Vreven, T.; Kudin, K. N.; Burant, J. C.; Millam, J. M.; Iyengar, S. S.; Tomasi, J.; Barone, V.; Mennucci, B.; Cossi, M.; Scalmani, G.; Rega, N.; Petersson, G. A.; Nakatsuji, H.; Hada, M.; Ehara, M.; Toyota, K.; Fukuda, R.; Hasegawa, J.; Ishida, M.; Nakajima, T.; Honda, Y.; Kitao, O.; Nakai, H.; Klene, M.; Li, X.; Knox, J. E.; Hratchian, H. P.; Cross, J. B.; Bakken, V.; Adamo, C.; Jaramillo, J.; Gomperts, R.; Stratmann, R. E.; Yazyev, O.; Austin, A. J.; Cammi, R.; Pomelli, C.; Ochterski, J. W.; Ayala, P. Y.; Morokuma, K.; Voth, G. A.; Salvador, P.; Dannenberg, J. J.;

Zakrzewski, V. G.; Dapprich, S.; Daniels, A. D.; Strain, M. C.; Farkas, O.; Malick, D. K.; Rabuck, A. D.; Raghavachari, K.; Foresman, J. B.; Ortiz, J. V.; Cui, Q.; Baboul, A. G.; Clifford, S.; Cioslowski, J.; Stefanov, B. B.; Liu, G.; Liashenko, A.; Piskorz, P.; Komaromi, I.; Martin, R. L.; Fox, D. J.; Keith, T.; Al-Laham, M. A.; Peng, C. Y.; Nanayakkara, A.; Challacombe, M.; Gill, P. M. W.; Johnson, B.; Chen, W.; Wong, M. W.; Gonzalez, C.; Pople, J. A. *Gaussian 03*, revision C.02; Gaussian, Inc.: Wallingford, CT, 2004.

(96) Harvey, J. N.; Aschi, M.; Schwarz, H.; Koch, W. *Theor. Chem. Acc.* **1998**, *99*, 95.

(97) Neese, F.; Petrenko, T.; Ganyushin, D.; Olbrich, G. *Coord. Chem. Rev.* **2007**, *251*, 288.

(98) Danovich, D.; Shaik, S. *J. Am. Chem. Soc.* **1997**, *119*, 1773.

(99) Weigend, F.; Ahlrichs, R. *Phys. Chem. Chem. Phys.* **2005**, *7*, 3297.

(100) Siegbahn, P. E. *Q. Rev. Biophys.* **2003**, *36*, 91.

(101) Neese, F. *J. Am. Chem. Soc.* **2006**, *128*, 10213.

(102) Pettersen, E. F.; Goddard, T. D.; Huang, C. C.; Couch, G. S.; Greenblatt, D. M.; Meng, E. C.; Ferrin, T. E. *J. Comput. Chem.* **2004**, *25*, 1605.

(103) Hodgkiss, J. M.; Nocera, D. G. Mechanistic studies of photo-induced proton-coupled electron transfer and oxygen atom transfer reactions in model systems. Ph.D. Thesis, Massachusetts Institute of Technology, Cambridge, MA, 2006.

(104) Fiedler, A.; Schröeder, D.; Shaik, S.; Schwarz, H. *J. Am. Chem. Soc.* **1994**, *116*, 10734.

(105) Oriedo, J. V. B.; Russell, D. H. *J. Am. Chem. Soc.* **1993**, *115*, 8376.

(106) Filatov, M.; Shaik, S. *J. Phys. Chem. A* **1998**, *102*, 3835.

(107) Li, D.; Huang, X.; Han, K.; Zhan, C.-G. *J. Am. Chem. Soc.* **2011**, *133*, 7416.

(108) It should be noted here that the spin inversion points obtained at the B3LYP level do not necessarily coincide with those obtained at the CASSCF level. It may increase the energy gap between sextet and quartet states at the CASSCF level. Therefore, the strength of the SOC matrix elements is expected to be larger than these values.

(109) Shiota, Y.; Suzuki, K.; Yoshizawa, K. *Organometallics* **2005**, *24*, 3532.

(110) Chang, C. J.; Chng, L. L.; Nocera, D. G. *J. Am. Chem. Soc.* **2003**, *125*, 1866.

(111) Newmyer, S. L.; Ortiz de Montellano, P. R. *J. Biol. Chem.* **1995**, *270*, 19430.

(112) Lewis, N. S.; Nocera, D. G. *Proc. Natl. Acad. Sci. U.S.A.* **2006**, *103*, 15729.

(113) Westlake, B. C.; Brennaman, M. K.; Concepcion, J. J.; Paul, J. J.; Bettis, S. E.; Hampton, S. D.; Miller, S. A.; Lebedeva, N. V.; Forbes, M. D. E.; Moran, A. M.; Meyer, T. J.; Papanikolas, J. M. *Proc. Natl. Acad. Sci. U.S.A.* **2011**, *108*, 8554.

(114) Cho, K.-B.; Carvajal, M. A.; Shaik, S. *J. Phys. Chem. B* **2009**, *113*, 336.

(115) Derat, E.; Shaik, S. *J. Am. Chem. Soc.* **2006**, *128*, 13940.

(116) Rosenthal, J.; Nocera, D. G. *Acc. Chem. Res.* **2007**, *40*, 543.

(117) Huynh, M. H.; Meyer, T. J. *Chem. Rev.* **2007**, *107*, 5004.

(118) Kumar, D.; Hirao, H.; Shaik, S.; Kozlowski, P. M. *J. Am. Chem. Soc.* **2006**, *128*, 16148.

(119) Wang, D.; Zheng, J.; Shaik, S.; Thiel, W. *J. Phys. Chem. B* **2008**, *112*, 5126.